



Short Communication

Ship emission of nitrous acid (HONO) and its impacts on the marine atmospheric oxidation chemistry



Lei Sun^{a,b,1}, Tianshu Chen^{a,1}, Ying Jiang^a, Yang Zhou^c, Lifang Sheng^c, Jintai Lin^d, Juan Li^a, Can Dong^a, Chen Wang^b, Xinfeng Wang^a, Qingzhu Zhang^a, Wenxing Wang^a, Likun Xue^{a,*}

^a Environment Research Institute, Shandong University, Qingdao, Shandong, China

^b School of Environmental Science & Engineering, Qilu University of Technology (Shandong Academy of Sciences), Ji'nan, Shandong, China

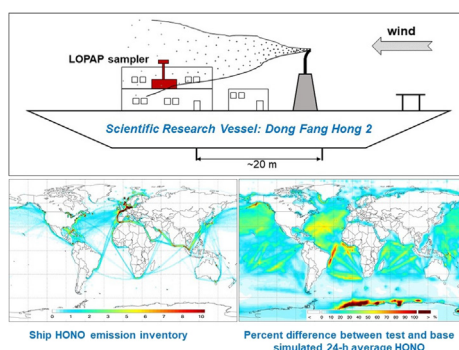
^c Key Laboratory of Physical Oceanography, College of Oceanic and Atmospheric Sciences, Ocean University of China, Qingdao, Shandong, China

^d Laboratory for Climate and Ocean-Atmosphere Studies, Department of Atmospheric and Oceanic Sciences, School of Physics, Peking University, Beijing, China

HIGHLIGHTS

- The ship emission ratio of $\Delta\text{HONO}/\Delta\text{NO}_x$ was measured for the first time during a cruise.
- A global HONO ship emission inventory was derived for use in chemical transport models.
- Ship emissions of HONO play an important role in the marine atmospheric oxidation processes.

GRAPHICAL ABSTRACT



ARTICLE INFO

Article history:

Received 8 February 2020

Received in revised form 9 May 2020

Accepted 9 May 2020

Available online 12 May 2020

Editor: Jianmin Chen

Keywords:

HONO

Ship emission

Emission inventory

OH

GEOS-Chem

ABSTRACT

Nitrous acid (HONO) is an important reservoir of the hydroxyl radical (OH) and thus plays a central role in tropospheric chemistry. Exhaust from engines has long been known as a major primary source of HONO, yet most previous studies focused on vehicle emissions on land. In comparison, ship emissions of HONO have been rarely characterized, and their impacts on the tropospheric oxidation chemistry have not been quantified. In this study, we conducted cruise measurements of HONO and related species over the East China Sea. Contrasting air masses from pristine marine background air to highly polluted ship plumes were encountered. The emission ratio of $\Delta\text{HONO}/\Delta\text{NO}_x$ ($0.51 \pm 0.18\%$) was derived from a large number of fresh ship plumes. Using the in-situ measured emission ratio, a global ship emission inventory of HONO was developed based on the international shipping emissions of NO_x in the Community Emission Data System inventory. The global shipping voyage emits approximately $63.9 \pm 22.2 \text{ Gg yr}^{-1}$ of HONO to the atmosphere. GEOS-Chem modelling with the addition of ship-emitted HONO showed that HONO concentrations could increase up to 40–100% over the navigation areas, leading to about 5–15% increases of primary OH production in the early-morning time. This study elucidates the potentially considerable effects of ship HONO emissions on the marine atmospheric chemistry, and calls for further studies to better characterize the ship emissions of HONO and other reactive species, which should be taken into account by global and regional models.

© 2020 Elsevier B.V. All rights reserved.

* Corresponding author.

E-mail address: xuelikun@sdu.edu.cn (L. Xue).

¹ These authors contributed equally to this work.

1. Introduction

Acting as a reservoir of the hydroxyl radical (OH), nitrous acid (HONO) plays a crucial role in the atmospheric photochemistry. Photolysis of HONO by sunlight produces an OH radical and a NO molecule, which initiate the atmospheric oxidation processes leading to formations of ozone (O₃) and secondary aerosols (Finlayson-Pitts and Pitts, 1999; Kleffmann, 2007). In the ambient atmosphere, HONO is either emitted from various primary sources such as combustion and microbial processes (Kurtenbach et al., 2001; Su et al., 2011), or formed by gas-phase and heterogeneous reactions involving nitrogen oxides (NO_x = NO + NO₂) (Finlayson-Pitts et al., 2003; George et al., 2005; Pagsberg et al., 1997). Recent studies have indicated that the sources of ambient HONO are rather complicated and have not yet been fully understood (Kleffmann et al., 2005; Stemmler et al., 2006; Zhou et al., 2011). Exploring the sources and environmental consequences of HONO is a fundamental step towards a better understanding of atmospheric chemistry, air pollution and climate change.

Exhaust of engine combustion is an important primary source of HONO in the atmosphere. In particular, vehicular exhaust has long been recognized as a major source of ambient HONO in urban areas (Pitts et al., 1984). In the recent decade, a number of field studies have measured the emission ratios of $\Delta\text{HONO}/\Delta\text{NO}_x$ from vehicles at tailpipe, tunnel and roadside in many metropolitan areas over the world (Kurtenbach et al., 2001; Li et al., 2018; Liu et al., 2017; Rappenglück et al., 2013; Xu et al., 2015; Yun et al., 2017). These studies have confirmed the significant contributions of vehicle emissions to the ambient HONO levels and hence atmospheric oxidizing capacity (Li et al., 2018; Xu et al., 2015). In comparison, little effort has been dedicated to characterize the emission factors of HONO from other transportation tools such as shipping vessels. Sea transport contributes to over 70% of the global trade by values and around 80% by volume, and at the beginning of 2015, the world's commercial fleet consisted of nearly 90,000 vessels according to the International Maritime Organization (<http://www.imo.org/en/Pages/Default.aspx>). Ships emit a large amount of air pollutants into the marine atmosphere, among which HONO is a highly reactive component. Ship emissions of HONO have high potential to perturb the atmospheric chemistry processes by supplying not only OH radicals but also NO_x, thus affect the marine atmosphere and climate change. To the best of our knowledge, the impacts of ship emissions of HONO on the marine atmosphere and climate have not been well quantified to date.

In the present study, we conducted cruise measurements of HONO and related species on the East China Sea. A large number of fresh ship plumes were encountered due to the vessel operation conditions, which provides a unique opportunity to characterize the emission factors of HONO from ship exhausts. In the following sections, we first show the overview of the measurement data and derive the $\Delta\text{HONO}/\Delta\text{NO}_x$ emission ratio from the ship plumes. We then develop a global ship emission inventory for HONO based on the measured emission ratio and the available NO_x ship emission database. Finally, a global chemical transport model (GEOS-Chem) is utilized to evaluate the impacts of ship emissions on HONO and OH radicals in the marine atmosphere. Overall, this study attempts to fill the knowledge gap of the ship emission of HONO and its effects on the marine atmosphere, and demonstrates the demand to further characterize the ship emissions of highly reactive air pollutants.

2. Methods

2.1. Field measurements

The cruise measurement campaign was conducted in the East China Sea (117–131°E, 23–33°N) from April 22 to May 27, 2017. The Scientific Research Vessel “Dong Fang Hong 2” was deployed

as the sampling platform. It is equipped with a medium speed diesel engine (MSDE; MAK 8M332C: 1380 KW and 900 RPM; gross tonnage = 3235) and fueled by relatively clean marine diesel oil (i.e., 0# diesel fuel), and has been in service for over twenty years for scientific research surveys in the China Sea (Zhang et al., 2017). According to the International Maritime Organization, the MSDE vessels account for about 21.1% of the total vessel fleet, similar to that of small-speed diesel engine vessels (20.1%) but slightly lower than that of high-speed diesel engine vessels (35.4%). The cabin housing the measurement instruments was located in the front of the funnel to eliminate potential interferences from ship plumes. We started the campaign when the vessel was far from the shore to avoid the impact of vehicle emissions and other sources at the port. In the present study, however, numerous stops were designed along the cruise route for collections of the air and sea water samples. During these stops, the air parcels sampled by the instruments in the cabin were frequently influenced by the freshly emitted ship plumes, which can be further confirmed by checking the concentration spikes of primary pollutants such as CO and NO_x. Therefore, the air masses sampled in the present study included not only marine air but also a lot of polluted ship plumes. A schematic diagram for the sampling of marine air and ship plume is shown in Fig. S1.

A package of commercial equipment was utilized for the field measurements of HONO and related species. Specifically, HONO was measured by a long path absorption photometer (LOPAP; QUMA GmbH) at a time resolution of 1 min (Kleffmann et al., 2002). Automatic zero checks using ultrapure nitrogen (purity of 99.999%) were performed regularly twice per day, and manual calibrations by nitrite standard solution were conducted every three days (Li et al., 2018). NO₂ was measured by a Cavity Attenuated Phase Shift (CAPS) spectroscopy instrument (Teledyne API, Model T500U), which is designed to be highly selective for NO₂ and free from possible interferences from other NO₂ species. NO and NO_y were measured by a chemiluminescence analyzer (Teledyne API, Model T200U), with an externally placed molybdenum oxide converter for the conversion of NO_y to NO. O₃ was measured by a UV photometric analyzer (TEI, Model 49C). CO was measured using a non-dispersive infrared analyzer (Teledyne API, Model 300EU) with automatic internal zero checks every 4 h. Particle number concentrations and size distribution in the range of 5–10,000 nm were measured by a Wide-range Particle Spectrometer (WPS; MSP Model 1000XP). J_{NO2} was measured by a filter radiometer (Meteorologie Consult GmbH). Meteorological parameters including temperature, relative humidity (RH), and winds were monitored by a commercial weather station. The measurement principles, accuracies, and quality assurance and control protocols for all of these instruments can be referred to Xue et al. (2016) and Li et al. (2018).

2.2. GEOS-Chem model

The GEOS-Chem global chemical transport model (Version 9-02) was used to simulate the impacts of ship HONO emissions on the global distributions of HONO and OH. The model was run with the standard HO_x-NO_x-VOC-O₃-aerosol chemistry (Mao et al., 2013) at a horizontal resolution of 2° × 2.5° with 47 vertical layers (including ten layers of ~0.13 km thickness below 850 hPa), as driven by the GEOS-FP assimilated meteorological fields. The global anthropogenic emissions were based on the Emission Database for Global Atmospheric Research (EDGAR) v4.2 inventory for CO and NO_x and Community Emission Data System (CEDS) for non-methane volatile organic compounds (NMVOCs) (Hoesly et al., 2018), which were further replaced by the regional inventories over Asia (INTEX-B), Europe (EMEP), Canada (CAC; http://www.ec.gc.ca/pdb/cac/cac_home_e.cfm) and China (MEIC; <http://www.meicmodel.org/>) (Auvray and Bey, 2005; Zhang et al., 2009). The international shipping emissions were adopted from the CEDS inventory, which has the updated fuel consumption that matches

the bottom-up estimates from the International Maritime Organization (2014), including monthly emissions of CO, NO_x, and SO₂ (Hoesly et al., 2018). Monthly biomass burning emissions were from the GFED3 inventory (van der Werf et al., 2010). Other natural emissions were parameterized base on the modelled meteorology. See Yan et al. (2016) for the detailed configurations of the model. The model was run with and without ship emissions of HONO, and differences between the two simulations are regarded as the effects of the ship-emitted HONO. Since the CEDS inventory has been updated to 2014 to reflect the actual emissions in recent years, we performed a half-year spin-up simulation and used the simulation results for July 2014 (summer scenario) for further analyses. Though inconsistent with the observation time period, the results of different sensitivity tests can represent potential impacts of ship HONO emissions on the marine atmospheric chemistry.

3. Results and discussion

3.1. Ship emission ratios of $\Delta\text{HONO}/\Delta\text{NO}_x$

The time series of measured air pollutants and weather conditions during the vessel cruise are shown in Fig. 1. Clearly, contrasting air masses from very clean marine background air to highly polluted air parcels were alternately encountered, as indicated by the significant variation in the concentration levels of primary pollutants such as NO_x. The fresh ship plumes and pristine marine background air were carefully selected for further analyses. The ship plumes were mainly sampled during the ship stops with obvious concentration spikes for primary pollutants (such as NO_x and HONO) but lower O₃ levels. Considering the absence of other pollution sources in the sea, such high levels of primary pollutants are believed to be due to the emissions of the research vessel. The detailed selection criteria of ship plumes include (a) only the data when the vessel stopped and the plume

moved through the sampling inlet were considered (Fig. S1); and (b) concentration spikes of HONO and NO_x as well as reduction in O₃ concentrations were observed. A total of 2751 min measurements were identified as the ship plume data, indicating the frequent influence of ship plumes. The averaged mixing ratios ($\pm\text{SD}$) of NO, NO₂ and HONO for the ship plumes were 73.6 ± 171 , 27.6 ± 22.4 and 0.39 ± 0.72 ppbv, with maximum values of 1767, 254 and 7.54 ppbv, respectively (see Table 1). The large range of SD values is mainly caused by the different engine loads during the ship voyage and the stopping time. The marine background air was sampled in the open sea far away from the coast, with extremely low levels of primary pollutants. The mean marine background concentrations ($\pm\text{SD}$) of NO, NO₂ and HONO were 20 ± 10 , 110 ± 40 and 2 ± 2 pptv, respectively. These values are representative of the global background conditions, and will be subtracted from the ship plume data to derive the $\Delta\text{HONO}/\Delta\text{NO}_x$ emission ratios.

We then deduced the emission ratio (ER) of $\Delta\text{HONO}/\Delta\text{NO}_x$ for the above identified fresh ship plumes. Based on the huge number of instantaneous ship plume data, the average ($\pm\text{SD}$) ER was $0.46 \pm 0.31\%$ with a median value of 0.41% (see Table 2). Furthermore, 90% of the individual ER values (i.e., 5–95% percentiles) are concentrated in the range of 0.08–0.97%. The scatter of ER values case by case should be due to the differences in the engine operation conditions and/or the ambient atmospheric conditions (e.g., age of plumes), which is also the case for the vehicle emission ratios on land (Xu et al., 2015). We also calculated the ER of $\Delta\text{HONO}/\Delta\text{NO}_x$ for the more strictly defined ship plumes, which should last for at least 15 min with concurrent high concentrations of HONO and NO_x. With this criterion, a total of 37 typical plumes were screened out, covering 1202 min measurement data. These plumes further removed the possible interference to the measurement data in short durations and ensured the high HONO and NO_x levels were indeed affected by the ship plumes. The averaged ($\pm\text{SD}$) ER for

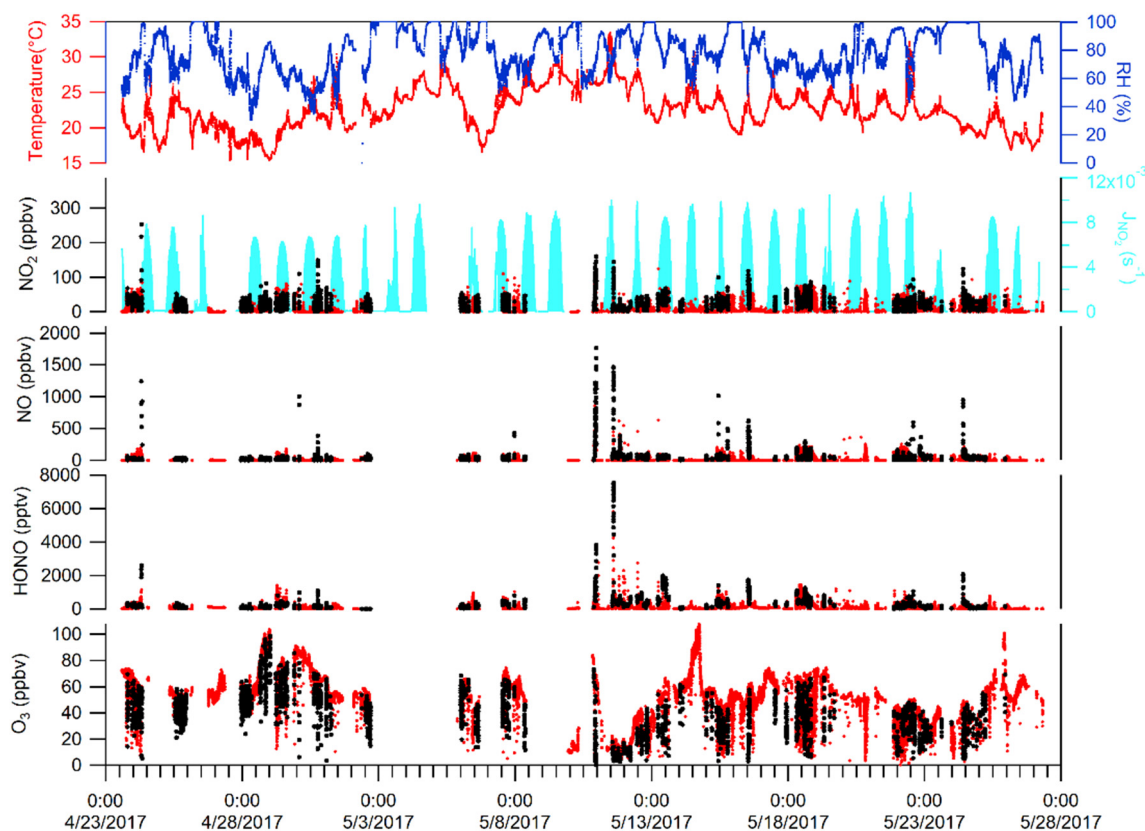


Fig. 1. Time series of measured species and meteorological parameters during the East China Sea voyage from April 22 to May 27, 2017. The black dots represent the ship plume data selected for analyses. Note that only data collected when the vessel stopped and the plume passing through the sampling inlet were selected as ship plumes in this study.

Table 1
Descriptive statistics of the measured mixing ratios of HONO and related species in the ship plumes and marine background air. Units are ppbv.

Species	Ship plume (N = 2751)				Marine background (N = 952)			
	Average	SD	Median	Max	Average	SD	Median	Max
NO	73.6	171	28.8	1767	0.02	0.01	0.02	0.04
NO ₂	27.6	22.4	22.9	254	0.11	0.04	0.12	0.17
HONO	0.39	0.72	2.02	7.54	0.002	0.002	0.002	0.002
CO	213	95	192	1157	81	49	100	118

Table 2
Emission ratios of $\Delta\text{HONO}/\Delta\text{NO}_x$ derived from all ship plume data and from typical ship plumes.

Parameter	All ship plume data (N = 2751)			Typical ship plume (N = 1202) ^a		
	ΔNO_x (ppb)	ΔHONO (ppb)	$\Delta\text{HONO}/\Delta\text{NO}_x$	ΔNO_x (ppb)	ΔHONO (ppb)	$\Delta\text{HONO}/\Delta\text{NO}_x$
Average	67	0.31	0.46%	79	0.43	0.51%
Median	48	0.19	0.41%	46	0.20	0.43%
Standard Deviation	124	0.69	0.31%	25	0.09	0.18%
Daytime Mean	84	0.44	0.53%	110	0.67	0.59%
Nighttime Mean	48	0.17	0.37%	47	0.18	0.42%

^a Typical ship plume refers to the plume that lasts for at least 15 min with concurrent data of HONO and NO_x at high concentrations. N denotes the number of minute data.

these typical plumes was calculated as $0.51 \pm 0.18\%$ with a median value of 0.43%, which are quite comparable to those derived from the instantaneous data case. In the following sections, the ER of 0.51% was adopted to derive the ship emission inventory of HONO, which can be considered as an overall average estimation of ship HONO emission.

An interesting finding is the discrepancy between the $\Delta\text{HONO}/\Delta\text{NO}_x$ ratios derived from the daytime and nighttime ship plumes. The ER derived from the daytime ship plume data (7:00–19:00 local time, LT; including 1447 min data) was $0.53\% \pm 0.37\%$, which is significantly higher than that ($0.37\% \pm 0.21\%$) obtained from the nighttime data (19:00–7:00 LT; containing 1304 min data) ($p < .01$). Fig. S2 (a) and S2(b) show that the $\Delta\text{HONO}/\Delta\text{NO}_x$ ratios generally increase with the measured J_{NO_2} levels, (except that J_{NO_2} value is in the range of $3\text{--}4 \times 10^{-3} \text{ s}^{-1}$), indicating the significant influence of the solar radiation. Therefore, the higher daytime $\Delta\text{HONO}/\Delta\text{NO}_x$ ratios should be attributed to the rapid photo-enhanced heterogeneous conversion of NO₂ to HONO on the surface of freshly-emitted particles such as soot. Laboratory studies have proposed the photo-enhanced uptake of NO₂ on aerosol surfaces as a potential daytime source of HONO (George et al., 2005; Monge et al., 2010), and our results provide the direct evidence of this process in the ambient atmosphere.

In general, the ocean-going vessels, such as container ships, cargo carriers and tankers, usually burn heavy fuel oil (HFO) in the open waters, which release more SO₂ and metals. Whereas in harbours or specific emission regulation areas, the ferries, bulk carriers, and other smaller ship mostly burn marine diesel oil (MDO) instead. Diesch et al. (2013) showed that the ship gross tonnage was directly proportional to the engine power. The emission ratios of NO_x of larger vessels (gross tonnage >30,000 tons) were 1.5 times higher than that of the smaller vessels (gross tonnage <5000 tons). In addition, Celik et al. (2020) pointed out that more efficient fuel combustion resulted in more NO_x emissions owing to the higher combustion temperature. Another important impact factor is fuel quality. According to Zhao et al. (2020), the emission of NO_x could be reduced by approximately 20% when the research vessel burned MDO instead of HFO under different engine loads. The research vessel in this study is a smaller vessel (gross tonnage = 3235 tons) and uses MDO as the fuel. Thus, we believe that the emission of NO_x under this circumstance is relatively low.

The ship emission related experimental studies can be performed in stationary platforms (at harbours or ports and mobile platforms in research vessels/aircrafts measurements), and in the exhaust funnels. Merico et al. (2016) reported the observed NO peak concentration of ~102 ppbv at the harbour area (50 m from the water), which was comparable to the NO levels in this study. In contrast, Zhao et al. (2020)

measured the emission gases directly from the chimney and the mean NO concentrations (MGO: 1438 ± 289 ppm; HFO: 1448 ± 272 ppm) were much higher than that found in this study. Table S1 compares our measured ship emission ratios of $\Delta\text{HONO}/\Delta\text{NO}_x$ against the results obtained for on-road vehicle emissions from many metropolitan areas in the world. The different values of ER implied the effects of other factors such as different types of engines, fuels, and working conditions on the HONO emissions in the real atmosphere (Huang et al., 2018; Kurtenbach et al., 2001). In general, the emission ratios derived in the present study are well within the reported range of ER for vehicle emissions (e.g., 0.10–1.70%), suggesting the similarity of HONO emission factors from engine exhaust. Thus, results in this study are representative of the emission ratios from ship engine exhausts. To improve the representativeness of this study, we divided the ER into three categories: 0.51% for this study; 1.7% for the maximum ratio and 0.03% for the minimum ratio.

3.2. A global ship HONO emission inventory

A global ship emission inventory of HONO was then developed based on the average in-situ measured ER of $\Delta\text{HONO}/\Delta\text{NO}_x$ (0.51%) and the CEDS ship emission inventory for NO_x (Hoesly et al., 2018). Fig. 2 shows the spatial distribution of ship HONO emissions. The ship-emitted HONO primarily concentrated over the navigation areas (i.e., the shipping routes and international ports), with much stronger emission intensity in the Northern Hemisphere. The estimated mean (\pm SD) annual emission of HONO from global shipping was $63.9 \pm 22.2 \text{ Gg yr}^{-1}$, which was much smaller than those of NO_x, SO₂ and CO. The Northwest Pacific (i.e., west of 180°E and north of 15°N), Northeast Pacific (i.e., east of 180°E and north of 15°N), Northern Atlantic (i.e., north of 15°N), Indian Ocean & Red Sea, and the Mediterranean & offshore areas of continental Europe are the major emission zones, with annual emissions of 8.1 ± 2.8 , 14.1 ± 4.9 , 24.7 ± 8.6 , 8.7 ± 3.0 , and $49.0 \pm 17.2 \text{ Gg yr}^{-1}$, respectively. Monthly emissions were also estimated and results are summarized in Table S2. Overall, the ship related HONO emissions in the second half of the year (July–December; $5.4\text{--}5.7 \text{ Gg mon}^{-1}$ with a total of $33.5 \pm 11.7 \text{ Gg}$) are slightly higher than those in the first half (January–June; $4.4\text{--}5.5 \text{ Gg mon}^{-1}$ with a total of $30.4 \pm 10.6 \text{ Gg}$). This pattern was the same as NO_x emissions, which reflects seasonal variations of in shipping business or other ship-related activities.

The HONO emission inventory derived this study is subject to large uncertainties. Potential uncertainties mainly arise from uncertainties of the HONO/NO_x emission ratio and the CEDS ship emission inventory

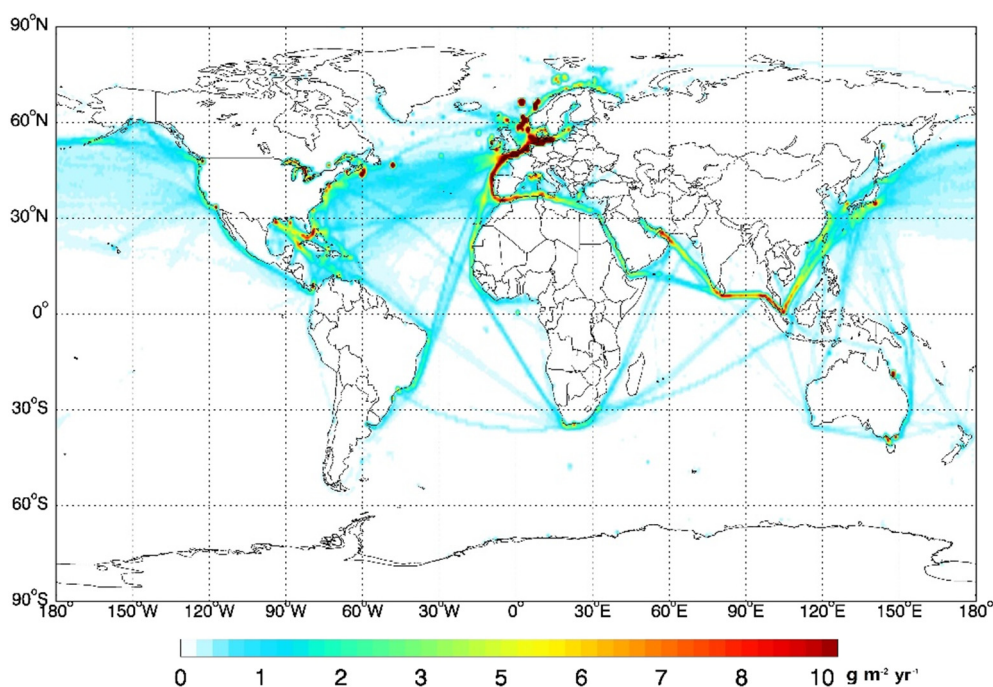


Fig. 2. Annual ship emission inventory of HONO ($\text{g m}^{-2} \text{yr}^{-1}$) developed by the measured emission ratio of $\Delta\text{HONO}/\Delta\text{NO}_x$ and the CEDS NO_x emissions in 2014. The grid resolution is $0.5^\circ \times 0.5^\circ$.

for NO_x . The emission ratio was derived from only one vessel despite a huge amount of ship plume data. Therefore, we estimated ship HONO emissions based on previous reported values of ER to improve its representativeness. The ship HONO emissions estimated from the maximum ratio (1.7%) and the minimum ratio (0.03%) of HONO/NO_x were listed in Table S2. In addition, the uncertainty of ship NO_x emissions may result from the uncertainties of the CEDS inventory as well. Hoesly et al. (2018) have shown that IEA-reported consumption is incomplete and additional fuel consumption is needed to match the bottom-up estimates from the International Maritime Organization in CEDS. However, more research is needed to improve the reliability of CEDS ship emission inventory. Furthermore, nearly 70% of the ship emissions occurred within 400 km of coastlines along the main trade routes (Corbett et al., 1999). Therefore, the global inventory may underestimate the emissions of short-distance ships near the continents. Despite these deficiencies, this first piece of ship emission inventory of HONO may still be considered by modelling studies before a more refined inventory is in place.

3.3. Impacts on the atmospheric oxidation processes

Influences of ship HONO emissions on the ambient HONO and OH radicals in the marine atmosphere were determined by the GEOS-Chem model. Model simulated meteorology (2-m temperature, relative humidity, and winds) was evaluated against the high qualities GEOS-FP output which uses the most recent validated GEOS system. Fig. S3 shows that the spatial distributions of different meteorological variables are comparable with the GEOS-FP output data. In addition, O_3 , NO_2 and HONO were evaluated against observational data. Fig. S4, Table S3 and S4 show that the model performed relatively well in reproducing the observed levels of O_3 and HONO. Fig. S5 shows that the model cannot capture observed high NO_2 , probably due to the low model resolution and the positive biases of the measurement (Sun et al., 2019; Xu et al., 2015). Overall, the model performed reasonably well in reproducing the HONO measurement. Fig. S6 shows the global distributions of HONO, OH, and primary OH sources (P_{OH} : the OH production rate from photolysis of HONO, O_3 , H_2O_2 , HNO_3 and OVOCs) as well as ozonolysis reactions of unsaturated VOCs) from the Base Scenario

without ship HONO emissions. The model predicted higher HONO levels in the polluted continental areas (e.g., East Asia and western Europe), with maximum values of 1–2 ppbv for Eastern China. Such levels are comparable to the in-situ determined concentrations in these continental regions (e.g., Li et al., 2018 and references therein). In comparison, the much lower HONO mixing ratios (i.e., 2.4–50 pptv with an average of 9.8 ± 8.8 pptv) simulated in the East China Sea and near ocean areas are actually higher than the measured values (2 ± 2 pptv for the marine background air) in this study. The overestimation of HONO is mostly due to the low model resolution, i.e., one grid may cover both coastal and offshore areas. For OH and P_{OH} , the model calculated higher levels in the polluted continents and their adjacent coastal regions, and moderate levels ($1\text{--}4 \times 10^6$ molecules cm^{-3} and $0.5\text{--}2 \times 10^6$ molecules $\text{cm}^{-3} \text{s}^{-1}$) in the vast oceans.

Figs. 3 and 4 presents the detailed impacts of ship emissions on the ambient 24-h average HONO and OH in the global marine atmospheres. With the inclusion of ship HONO emissions, the model predicts significant enhancements of HONO concentrations in the navigation areas. The enhancements in the absolute concentration of HONO reach up to 10 pptv in the North Sea, 3 pptv in the east of North America and are about 0.5–1.5 pptv in the Northwest Pacific, Northeast Pacific, North Atlantic, Red Sea and some famous seaports. Generally, the enhancements of HONO in percentage are 40–100% along the major shipping routes. This indicates ship emission presents a major source of HONO in the global marine atmosphere. HONO concentration enhancements mostly occurred in the nighttime, reaching up to 80–100% in the major shipping routes (Fig. S7). In comparison, the enhancement was much lower during the daytime due to the fast photolysis.

As HONO photolysis is a major source of OH, ship emissions of HONO could serve as an additional OH supplier and hence enhance the atmospheric oxidation processes. Our modelling results showed an enhancement of 20–40% in the OH production rate from HONO photolysis over the majority of shipping routes after including shipping emissions (Fig. S8). As shown in Fig. 4a and b, ship emissions of HONO also resulted in significant increases (i.e., $1\text{--}4 \times 10^4$ molecules $\text{cm}^{-3} \text{s}^{-1}$ or 5–15% in percentage) of the total primary source of OH (P_{OH}) in the navigation areas during the early morning period (6:00–7:00 LT). This suggests that ship-emitted HONO may play an important role in the jump

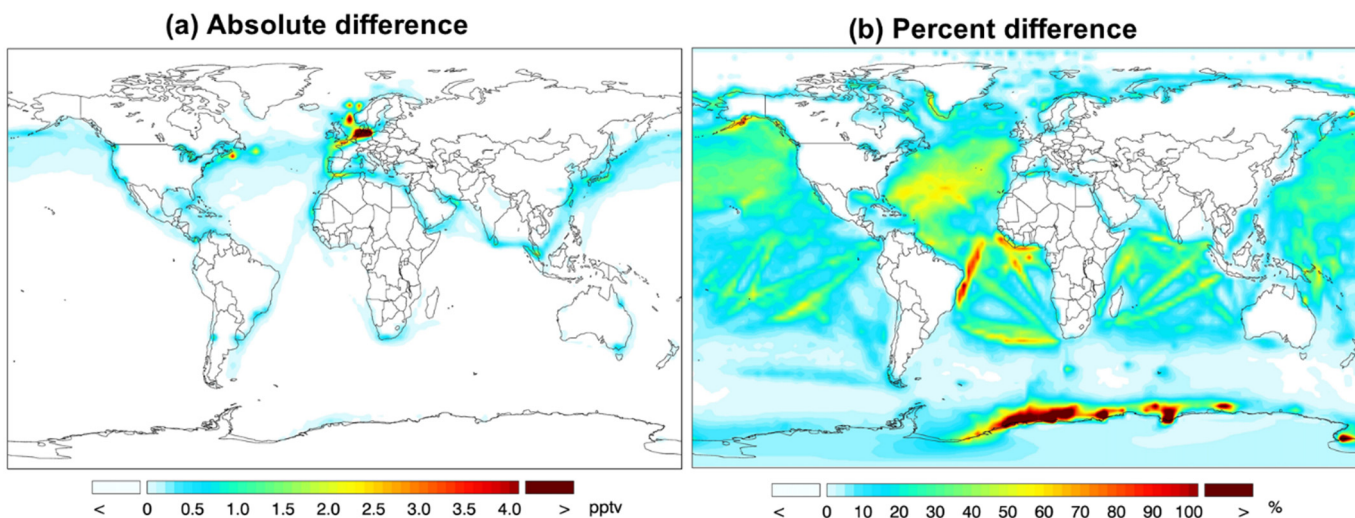


Fig. 3. Absolute and percent differences between Test (standard emissions + ship HONO emissions) and Base (standard emissions) simulated 24-h average HONO in July 2014. The absolute difference represents the value of Test minus Base simulation (Test-Base), and the percent difference represents (Test-Base)/Base*100%.

start of the atmospheric photochemistry in the marine atmosphere. In comparison, the impact of ship-emitted HONO on OH production is minor during the daytime (Fig. S9), indicating that OH productions are dominated by other pathways (i.e. HO₂ + NO and so on), and the accumulation of HONO during the nighttime has been photolyzed at dawn. We also examined the impacts of ship HONO emissions on the tropospheric O₃ in the marine atmosphere, and found that they are almost negligible (<1%; figures not shown). This is because O₃ formation is NO_x-limited in the pristine marine atmosphere, and adding OH radicals is insensitive to O₃ formation and might even lead to O₃ destruction via the O₃ + HO_x reaction cycles. In order to improve the representativeness of the simulation results, two sensitivity tests were performed by setting the ER to 1.7% and 0.03%, representing the maximum and minimum ratios in ship plume, respectively (according to the literature results in Table S2). The two test results showed significant differences. HONO concentration reached up to 40 pptv in the North Sea and 100–200% over the major shipping routes when we set ER to 1.7% (Fig. S10(a) and S10(b)). Similarly, the ship HONO emissions promoted the OH production, which increased 3–10 × 10⁴ molecules cm⁻³ s⁻¹ or 20–40% for the P_{OH} (Fig. S11). However, when ER was set to 0.03%, HONO concentrations and P_{OH} did not show much difference, suggesting the impacts can be ignored.

The aforementioned analyses elucidate the significant contributions of ship emissions to the ambient HONO and OH sources in the marine air. Once OH is produced, it immediately involves in the atmospheric oxidation cycles and oxidizes a variety of reduced substances such as VOCs and DMS. One should keep in mind that the present analysis may be subject to some uncertainty due to limitations of the methodology data representativeness. Nevertheless, we believe that the current estimation should represent a lower limit for the importance of ship HONO emissions given the following reasons. First, as mentioned above, the CEDS emission may not cover all the shipping vessels, especially for those with short travel voyages (Hoesly et al., 2018; Liu et al., 2016). Second, the marine diesel oil used by the research vessel in this study is a typical clean fuel and emits relatively low levels of air pollutants compared to common cargo ships. Third, our analysis suggests the additional formation of HONO from the heterogeneous reactions of NO₂ on the surface of particles, both of which are major constituents of ship emissions, and this process was not considered in the GEOS-Chem simulations. Obviously, more efforts are urgently needed to test more ships, fuels, operation conditions, etc., and to compile more accurate ship emission inventories for a better understanding of the influences of global shipping on the marine atmosphere and climate.

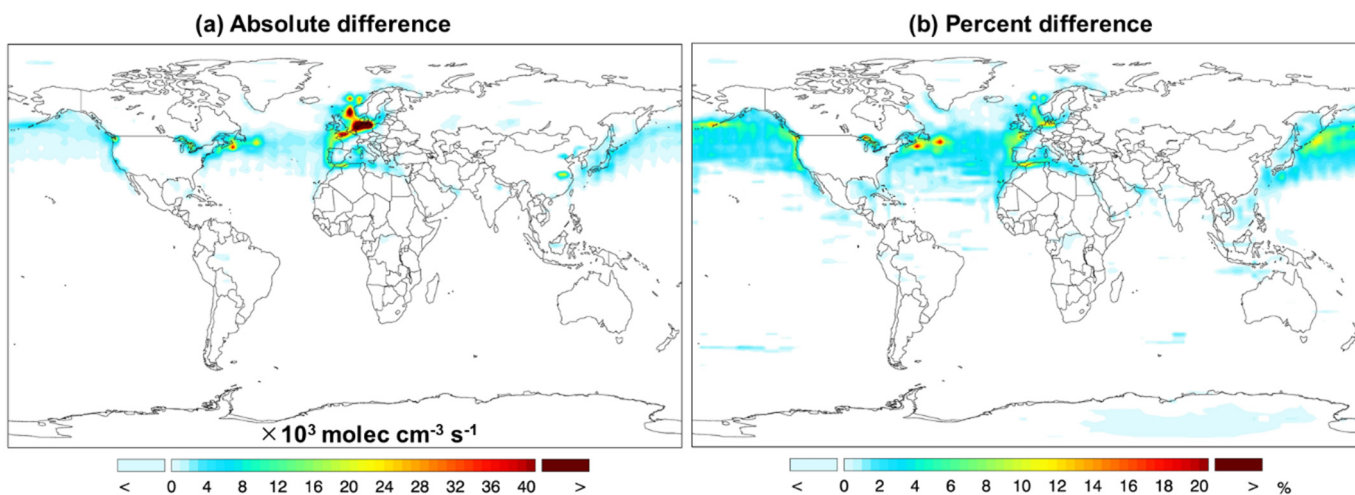


Fig. 4. Absolute and percent differences between Test and Base simulated total primary OH sources (P_{OH}) during the early morning time (6:00–7:00 LT). We converted the UTC time to the local time according to the time zone, i.e., every 15° longitude represents 1 h.

4. Summary

We present the direct measurements of emission ratio of $\Delta\text{HONO}/\Delta\text{NO}_x$ from a large number of fresh ship plumes. A global ship emission inventory of HONO was compiled for the first time based on the measured emission ratio and the available emission data for NO_x , and is ready for use in chemical transport models. GEOS-Chem modelling analysis illustrates the potentially important impacts of ship emissions on ambient HONO, primary OH sources, and thus oxidation capacity in the marine atmosphere. Despite the inherent uncertainty from the field measurements and ship emission database, this study is a good initiative to revisit the roles of ship emissions in the marine atmospheric chemistry. Further studies are urgently needed to better characterize the ship emissions of HONO and other reactive species and to thoroughly evaluate their impacts on atmospheric chemistry and climate change.

CRedit authorship contribution statement

Lei Sun: Formal analysis, Writing - original draft. **Tianshu Chen:** Investigation, Data curation, Formal analysis. **Ying Jiang:** Investigation, Data curation. **Yang Zhou:** Investigation, Resources. **Lifang Sheng:** Investigation, Resources, Writing - review & editing. **Jintai Lin:** Supervision, Writing - review & editing. **Juan Li:** Investigation. **Can Dong:** Writing - review & editing. **Chen Wang:** Writing - review & editing. **Xinfeng Wang:** Investigation. **Qingzhu Zhang:** Writing - review & editing. **Wenxing Wang:** Supervision, Resources. **Likun Xue:** Conceptualization, Funding acquisition, Project administration, Writing - original draft.

Declaration of competing interest

The authors declare that they have no known competing financial interests or personal relationships that could have appeared to influence the work reported in this paper.

Acknowledgements

This work was funded by the National Natural Science Foundation of China (Project No.: 91544213, 41505111 and 41922051), Shandong Provincial Science Foundation for Distinguished Young Scholars (ZR2019JQ09), the Qilu Youth Talent Program of Shandong University, the Jiangsu Collaborative Innovation Center for Climate Change, the Taishan Scholars (ts201712003) and the Young Scientist Cooperation Fund of Qilu University of Technology (Shandong Academy of Sciences) (Grant No. 2017BSHZ020). We appreciate Penggang Zheng and Rui Li for their help in setting up the instruments. The model simulations were performed at the Supercomputing Center of Shandong University in Weihai.

Appendix A. Supplementary data

Supplementary data to this article can be found online at <https://doi.org/10.1016/j.scitotenv.2020.139355>.

References

Auvray, M., Bey, I., 2005. Long-range transport to Europe: seasonal variations and implications for the European ozone budget. *J. Geophys. Res. Atmos.* 110, D11303. <https://doi.org/10.1029/2004JD005503>.

Celik, S., Drewnick, F., Fachinger, F., Brooks, J., Darbyshire, E., Coe, H., Paris, J.D., Eger, P.G., Schuladen, J., Tadic, I., Friedrich, N., Dienhart, D., Hottmann, B., Fischer, H., Crowley, J.N., Harder, H., Borrmann, S., 2020. Influence of vessel characteristics and atmospheric processes on the gas and particle phase of ship emission plumes: in situ measurements in the Mediterranean Sea and around the Arabian peninsula. *Atmos. Chem. Phys.* 20, 4713–4734.

Corbett, J.J., Fischbeck, P.S., Pandis, S.N., 1999. Global nitrogen and sulfur inventories for oceangoing ships. *J. Geophys. Res. Atmos.* 104, 3457–3470.

Diesch, J.M., Drewnick, F., Klimach, T., Borrmann, S., 2013. Investigation of gaseous and particulate emissions from various marine vessel types measured on the banks of the Elbe in northern Germany. *Atmos. Chem. Phys.* 13, 3603–3618.

Finlayson-Pitts, B.J., Pitts Jr., J.N., 1999. *Chemistry of the Upper and Lower Atmosphere: Theory, Experiments, and Applications*. Academic, San Diego, California.

Finlayson-Pitts, B., Wingen, L., Sumner, A., Syomin, D., Ramazan, K., 2003. The heterogeneous hydrolysis of NO_2 in laboratory systems and in outdoor and indoor atmospheres: an integrated mechanism. *Phys. Chem. Chem. Phys.* 5, 223–242.

George, C., Strekowski, R., Kleffmann, J., Stemmler, K., Ammann, M., 2005. Photoenhanced uptake of gaseous NO_2 on solid organic compounds: a photochemical source of HONO? *Faraday Discuss.* 130, 195–210.

Hoesly, R.M., Smith, S.J., Feng, L., Klimont, Z., Janssens-Maenhout, G., Pitkanen, T., Seibert, J.J., Vu, L., Andres, R.J., Bolt, R.M., Bond, T.C., Dawidowski, L., Kholod, N., Kurokawa, J.I., Li, M., Liu, L., Lu, Z., Moura, M.C.P., O'Rourke, P.R., Zhang, Q., 2018. Historical (1750–2014) anthropogenic emissions of reactive gases and aerosols from the community emissions data system (CEDS). *Geosci. Model Dev.* 11, 369–408.

Huang, C., Hu, Q., Wang, H., Qiao, L., Jing, S.a., Wang, H., Zhou, M., Zhu, S., Ma, Y., Lou, S., Li, L., Tao, S., Li, Y., Lou, D., 2018. Emission factors of particulate and gaseous compounds from a large cargo vessel operated under real-world conditions. *Environ. Pollut.* 242, 667–674.

Kleffmann, J., 2007. Daytime sources of nitrous acid (HONO) in the atmospheric boundary layer. *ChemPhysChem* 8, 1137–1144.

Kleffmann, J., Heland, J., Kurtenbach, R., Lörzer, J.C., Wiesen, P., 2002. A new instrument (LOPAP) for the detection of nitrous acid (HONO). *Environ. Sci. Pollut. R.* 9 (4), 48–54 (special issue).

Kleffmann, J., Gavriloaiei, T., Hofzumahaus, A., Holland, F., Koppmann, R., Rupp, L., Schlosser, E., Siese, M., Wahner, A., 2005. Daytime formation of nitrous acid: a major source of OH radicals in a forest. *Geophys. Res. Lett.* 32, L05818.

Kurtenbach, R., Becker, K.H., Gomes, J.A.G., Kleffmann, J., Lörzer, J.C., Spittler, M., Wiesen, P., Ackermann, R., Geyer, A., Platt, U., 2001. Investigations of emissions and heterogeneous formation of HONO in a road traffic tunnel. *Atmos. Environ.* 35, 3385–3394.

Li, D., Xue, L., Wen, L., Wang, X., Chen, T., Mellouki, A., Chen, J., Wang, W., 2018. Characteristics and sources of nitrous acid in an urban atmosphere of northern China: results from 1-yr continuous observations. *Atmos. Environ.* 182, 296–306.

Liu, H., Fu, M., Jin, X., Shang, Y., Shindell, D., Faluvegi, G., Shindell, C., He, K., 2016. Health and climate impacts of ocean-going vessels in East Asia. *Nat. Clim. Chang.* 6, 1037.

Liu, Y., Lu, K., Ma, Y., Yang, X., Zhang, W., Wu, Y., Peng, J., Shuai, S., Hu, M., Zhang, Y., 2017. Direct emission of nitrous acid (HONO) from gasoline cars in China determined by vehicle chassis dynamometer experiments. *Atmos. Environ.* 169, 89–96.

Mao, J., Paulot, F., Jacob, D.J., Cohen, R.C., Crouse, J.D., Wennberg, P.O., Keller, C.A., Hudman, R.C., Barkley, M.P., Horowitz, L.W., 2013. Ozone and organic nitrates over the eastern United States: sensitivity to isoprene chemistry. *J. Geophys. Res. Atmos.* 118, 11,256–11,268.

Merico, E., Donato, A., Gambaro, A., Cesari, D., Gregoris, E., Barbaro, E., Dinoi, A., Giovanelli, G., Masieri, S., Contini, D., 2016. Influence of in-port ships emissions to gaseous atmospheric pollutants and to particulate matter of different sizes in a Mediterranean harbour in Italy. *Atmos. Environ.* 139, 1–10.

Monge, M.E., D'Anna, B., Mazzi, L., Giroir-Fendler, A., Ammann, M., Donaldson, D., George, C., 2010. Light changes the atmospheric reactivity of soot. *Proc. Natl. Acad. Sci. U. S. A.* 107, 6605–6609.

Pagsberg, P., Bjergbakke, E., Ratajczak, E., Sillesen, A., 1997. Kinetics of the gas phase reaction $\text{OH} + \text{NO} (+\text{M}) \rightarrow \text{HONO} (+\text{M})$ and the determination of the UV absorption cross sections of HONO. *Chem. Phys. Lett.* 272, 383–390.

Pitts, J.N., Biermann, H.W., Winer, A.M., Tuazon, E.C., 1984. Spectroscopic identification and measurement of gaseous nitrous acid in dilute auto exhaust. *Atmos. Environ.* 18 (1967), 847–854.

Rappenglück, B., Lubertino, G., Alvarez, S., Golovko, J., Czader, B., Ackermann, L., 2013. Radical precursors and related species from traffic as observed and modeled at an urban highway junction. *J. Air Waste Manage. Assoc.* 63, 1270–1286.

Stemmler, K., Ammann, M., Donders, C., Kleffmann, J., George, C., 2006. Photosensitized reduction of nitrogen dioxide on humic acid as a source of nitrous acid. *Nature* 440 (7081), 195–198.

Su, H., Cheng, Y., Oswald, R., Behrendt, T., Trebs, I., Meixner, F.X., Andreae, M.O., Cheng, P., Zhang, Y., Pöschl, U., 2011. Soil nitrate as a source of atmospheric HONO and OH radicals. *Science* 333, 1616–1618.

Sun, L., Xue, L., Wang, Y., Li, L., Lin, J., Ni, R., Yan, Y., Chen, L., Li, J., Zhang, Q., Wang, W., 2019. Impacts of meteorology and emissions on summertime surface ozone increases over central eastern China between 2003 and 2015. *Atmos. Chem. Phys.* 19, 1455–1469.

van der Werf, G.R., Randerson, J.T., Giglio, L., Collatz, G.J., Mu, M., Kasibhatla, P.S., Morton, D.C., DeFries, R.S., Jin, Y., van Leeuwen, T.T., 2010. Global fire emissions and the contribution of deforestation, savanna, forest, agricultural, and peat fires (1997–2009). *Atmos. Chem. Phys.* 10, 11707–11735.

Xu, Z., Wang, T., Wu, J., Xue, L., Chan, J., Zha, Q., Zhou, S., Louie, P.K.K., Luk, C.W.Y., 2015. Nitrous acid (HONO) in a polluted subtropical atmosphere: seasonal variability, direct vehicle emissions and heterogeneous production at ground surface. *Atmos. Environ.* 106, 100–109.

Xue, L., Gu, R., Wang, T., Wang, X., Saunders, S., Blake, D., Louie, P.K., Luk, C.W., Simpson, I., Xu, Z., 2016. Oxidative capacity and radical chemistry in the polluted atmosphere of Hong Kong and Pearl River Delta region: analysis of a severe photochemical smog episode. *Atmos. Chem. Phys.* 16, 9891–9903.

Yan, Y., Lin, J., Chen, J., Hu, L., 2016. Improved simulation of tropospheric ozone by a global-multi-regional two-way coupling model system. *Atmos. Chem. Phys.* 16, 2381–2400.

- Yun, H., Wang, Z., Zha, Q., Wang, W., Xue, L., Zhang, L., Li, Q., Cui, L., Lee, S., Poon, S.C., 2017. Nitrous acid in a street canyon environment: sources and contributions to local oxidation capacity. *Atmos. Environ.* 167, 223–234.
- Zhang, Q., Streets, D.G., Carmichael, G.R., He, K., Huo, H., Kannari, A., Klimont, Z., Park, I., Reddy, S., Fu, J., 2009. Asian emissions in 2006 for the NASA INTEX-B mission. *Atmos. Chem. Phys.* 9, 5131–5153.
- Zhang, Y., Yang, X., Brown, R., Yang, L., Morawska, L., Ristovski, Z., Fu, Q., Huang, C., 2017. Shipping emissions and their impacts on air quality in China. *Sci. Total Environ.* 581, 186–198.
- Zhao, J., Zhang, Y., Yang, Z., Liu, Y., Peng, S., Hong, N., Hu, J., Wang, T., Mao, H., 2020. A comprehensive study of particulate and gaseous emissions characterization from an ocean-going cargo vessel under different operating conditions. *Atmos. Environ.* 223, 117286.
- Zhou, X., Zhang, N., TerAvest, M., Tang, D., Hou, J., Bertman, S., Alaghmand, M., Shepson, P.B., Carroll, M.A., Griffith, S., 2011. Nitric acid photolysis on forest canopy surface as a source for tropospheric nitrous acid. *Nat. Geosci.* 4 (7), 440–443.